Appl. Phys. B 78, 791–795 (2004)
DOI: 10.1007/s00340-004-1472-z

Applied Physics B
Lasers and Optics

Z.-D. SUN[1]
Q. LIU[1]
R.M. LEES[1,✉]
L.-H. XU[1]
M.Y. TRETYAKOV[2]
V.V. DOROVSKIKH[2]

Saturation-dip measurements in the $2\nu_2$ overtone band of OCS with a CO_2-laser/microwave-sideband spectrometer

[1] Canadian Institute for Photonic Innovations and Department of Physical Sciences, University of New Brunswick, Saint John, N. B., Canada E2L 4L5
[2] Institute of Applied Physics of Russian Academy of Sciences, 46 Ulianov Str., Nizhnii Novgorod, 603950, Russia

Received: 3 December 2003
Published online: 30 March 2004 •

ABSTRACT We have employed a CO_2-laser/microwave-sideband spectrometer to carry out saturation-dip sub-Doppler measurements of a number of $2\nu_2$ overtone transitions of OCS in the 10-μm region. The OCS frequencies have been obtained with an absolute accuracy of order ±37 kHz, as determined from a careful analysis of the combined uncertainties in the frequency of our Lamb-dip-locked laser and the centers of the observed OCS saturation signals. Our ±37 kHz measurement accuracy is consistent with literature OCS sub-Doppler data obtained on a similar instrument. The results serve to extend the comb of precise reference frequencies in the 10-μm region and to determine the magnitudes of systematic and random uncertainties of our CO_2 laser.

PACS 07.57.Ty; 33.20.Ea; 42.62.Fi

1 Introduction

Recently, we have constructed a CO_2-laser/microwave-sideband (CO_2-MWSB) spectrometer with capability for saturation-dip sub-Doppler precision measurements in the 10-μm infrared region [1]. The instrument employs a CO_2-MWSB tunable source [2] with an Evenson CO_2 laser [3] and a Cheo waveguide modulator [4]. Tunable infrared radiation can be generated within sideband windows from 6.7–18.5 GHz on either side of each CO_2 laser line, not only for the regular 9.6 and 10.6 μm CO_2 laser bands but for many of the lines of the hot and sequence bands as well [1–3]. The $2\nu_2$ overtone band of OCS is accessible with our system, and provides a useful testing ground for checking our absolute measurement accuracy by comparison with a previous sub-Doppler study by Fichoux et al. in 1998 [5]. Our new measurements add to the data set of precise frequencies for the OCS $2\nu_2$ overtone band and extend the comb of known reference frequencies in the important 10-μm region. In this paper, we discuss the performance of our system in the context of the OCS measurements, and present our new data for the $2\nu_2$ transitions.

The linear OCS molecule with its simple spectrum is well recognized as a good calibration standard. In their 1991 compilation of reference data, Maki and Wells presented a large number of transition wavenumbers for the $2\nu_2$ overtone band and the $3\nu_2 - \nu_2$ hot band as determined from Doppler-limited infrared heterodyne measurements [6]. In 1998, Fichoux et al. measured seven saturation-dip frequencies for the $2\nu_2$ band and 13 for the $3\nu_2 - \nu_2$ band with a reported accuracy of ±20 kHz, employing a CO_2-MWSB spectrometer with 12–18 GHz sideband MW windows [5]. They also predicted complete sets of frequencies for these two bands to an accuracy of 10^{-6} cm^{-1} from a global analysis using energy expansions up to the eighth order in powers of $J(J+1)$. In the present study, we have extended the saturation-dip data set to include 16 further transitions in the $2\nu_2$ band. From a careful assessment of the measurement uncertainties in our system, we have determined the absolute accuracy of these new frequencies to be of order ±37 kHz, and have checked this result by performing comparative test measurements on previously known transitions.

2 Experimental details

The experimental setup for the sub-Doppler mode of our sideband spectrometer is illustrated in Fig. 1. Detailed descriptions of the instrument and the operating conditions have been presented in [1, 2].

About 20% of the CO_2 laser power is split off by beamsplitter BS1 and used for locking the laser. The locking beam is sent through an external CO_2 cell and reflected back by mirror M5 in order to produce a Lamb dip in the 4.3-μm fluorescence [7]. A first-derivative error-correction signal is obtained by frequency modulating the laser with a 1 kHz sinusoidal voltage applied to the piezoelectric tube on which the rear laser mirror is mounted. With a CO_2 pressure of about 40 mTorr in the fluorescence cell, an angle of 1.5 mrad between the counter-propagating locking beams, and a peak-to-peak modulation voltage of 0.6 V, the width of the Lamb dip is less than 1 MHz, as illustrated in [2] and discussed below in Sect. 4.

The power delivered in the main 80% beam to the Cheo electro-optic modulator varies from about 8 W for the stronger CO_2 laser lines down to about 1 W for the hot and sequence band lines and the high-J regular band lines. Microwave power of ∼ 15 W is supplied to the modulator from a traveling-wave-tube amplifier (TWTA) driven by a MW

✉ Fax: +1-506/648-5948, E-mail: lees@unb.ca

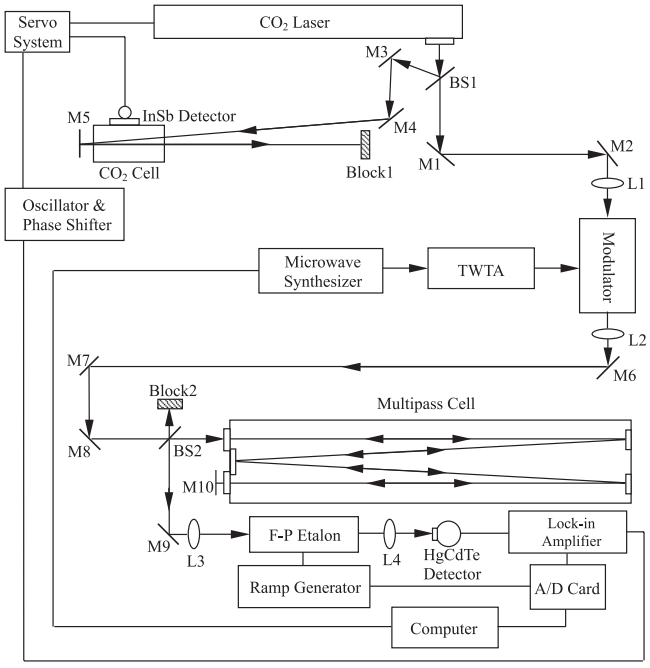

FIGURE 1 Block diagram of the tunable CO_2-laser/microwave-sideband spectrometer set up for high-resolution saturation-dip observations. BS1, BS2, beam splitters; L1, L2, ZnSe lenses; M1–M12, mirrors; TWTA, traveling wave tube amplifier; F–P, tunable Fabry–Pérot etalon filter

synthesizer, generating tunable sidebands on either side of the main CO_2 carrier. For the measurement of an OCS Lamb-dip, the synthesizer sweeps the frequency of the appropriate sideband over a narrow region containing the OCS absorption. With a measured 25% transmission efficiency for the modulator and a sideband conversion efficiency of $\sim 0.6\%$, we obtain a power of the order of 10 mW in each sideband at the output of the modulator for the stronger CO_2 laser lines.

In order to saturate the OCS transitions, the full modulator output is focused through beamsplitter BS2 in Fig. 1 into our multipass White-type absorption cell. This is of base length 0.6 m, and was set to 16 transits to give a total absorption path of 9.6 m. The radiation is retro-reflected by mirror M10 at the cell exit window in order to generate a counter-propagating beam inside the cell for observation of the OCS saturation dips. When the return beam re-emerges from the cell, it is reflected off BS2 and focused through a tunable Fabry–Pérot etalon filter that selects the desired sideband containing the OCS absorption signal. The saturation-dip signal is detected by a liquid-N_2-cooled HgCdTe detector and demodulated by a digital lock-in amplifier operating in $2f$-detection mode. We take advantage of the same 1 kHz modulation already present for the laser locking in order to produce the frequency-modulated saturation-dip spectral signal. This signal is then sent through an A/D card to the computer.

The microwave synthesizer frequency and power output, the ramp generator controlling the F–P filter, and the data acquisition are all computer-controlled by a program written in Visual C^{++}. A versatile object-oriented approach is utilized in the program that can control each device separately as well as provide total control of the experiment.

3 Sub-Doppler OCS measurements

Prior to the experiment, we looked through the known data and predictions for the $2\nu_2$ overtone band of OCS [5, 6] to determine the set of transitions that would fall within the tuning range of our spectrometer. Before each transition measurement, we set up a 3-MHz scan window centered on the predicted OCS frequency, and optimized the sideband power by adjusting the tuning of the F–P filter from the computer keyboard [1]. We then scanned through the OCS line, using a step size of 10 kHz, and recorded the saturation-dip signal on the computer. For each line, we measured the signal several times, scanning upwards and downwards. Figure 2 is a typical result showing the second-derivative $2f$ recording of the saturated absorption for the $P(16)$ OCS transition in the $2\nu_2$ band. Model line shapes (solid curves) were fitted by least squares to the data points (open circles) for a Gaus-

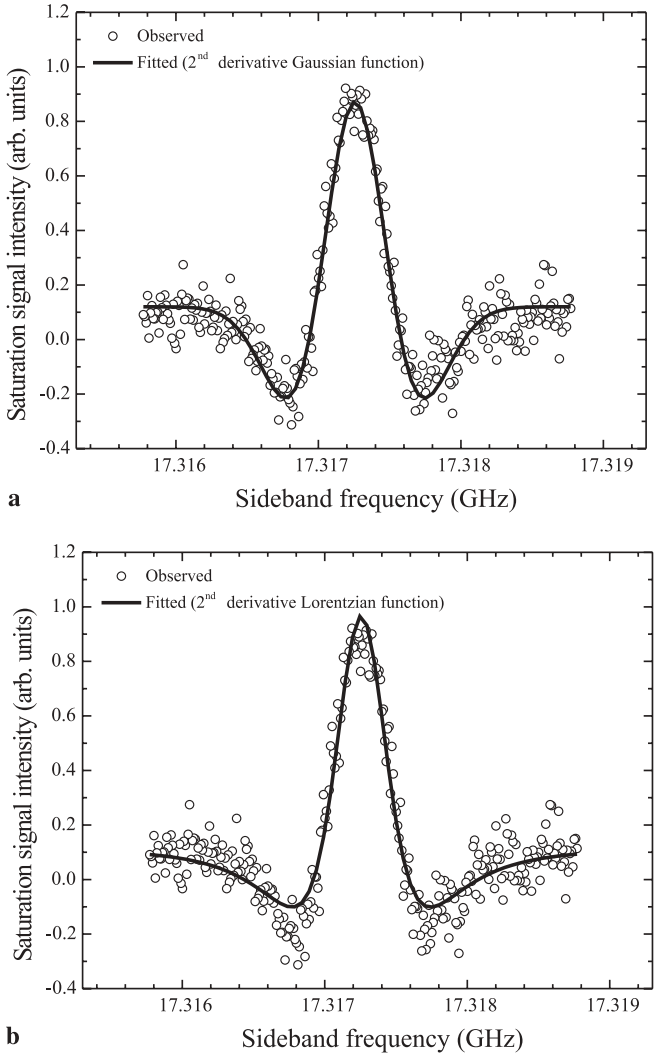

FIGURE 2 Saturation-dip signal for the $P(16)$ line of the $2\nu_2$ band of OCS, recorded using the lower sideband of the $9P(26)$ CO_2 laser line with the lock-in amplifier in $2f$ detection mode. The lock-in time constant was 30 ms and the OCS pressure was 8 mTorr. The *curves (solid lines)* represent least-squares fits of second-derivative line shapes to the experimental points *(open circles)* (**a**) an assumed Gaussian profile, and (**b**) an assumed Lorentzian profile

sian second-derivative profile in Fig. 2a and a Lorentzian in Fig. 2b. The fits were performed using Origin software using a second-derivative line shape function with adjustable height, center frequency and width plus an adjustable constant for the baseline.

The Gaussian line shape appears to fit the data better than the Lorentzian in Fig. 2, judging from the fit residuals, possibly due to a surviving contribution from Doppler broadening arising from curvature of the beam wavefronts in the multipass absorption cell, as suggested by G. Duxbury [8]. However, the fits to both lineshapes yielded essentially the same center frequency of 17 317.243 MHz with a standard deviation of ~ 5 kHz. The fitted FWHM (full-width at half-maximum) linewidth was approximately 650 kHz for the Gaussian profile in Fig. 2a. The specific form of the Gaussian lineshape expression that we used for Fig. 2a was

$$G(\nu) = G_o + A[2/\pi\Delta\nu_{pp}^2]^{1/2}\exp[-2(\nu-\nu_o)^2/\Delta\nu_{pp}^2] \qquad (1)$$

where ν_o is the center frequency, A is the integrated intensity, G_o is the baseline constant, and $\Delta\nu_{pp}$ is the frequency separation between the positive and negative peaks of the first derivative, $G'(\nu)$. For this form, the Gaussian FWHM is given by $[2\ln 2]^{1/2}\Delta\nu_{pp}$.

Altogether, we carried out saturation-dip frequency measurements for 21 OCS $2\nu_2$ lines, including 5 for which Lamb-dip measurements had previously been reported by Fichoux et al. [5]. Our results are listed in Table 1, with each frequency representing an average of from 3 to 7 up-and-down scans. The last column in Table 1 shows the differences between our experimental frequencies and the measured values given in [5].

OCS Transition	CO_2 Laser $\pm\nu_o$[a] (MHz)	ν_{obs}[b] (MHz)	$\Delta\nu$[c] (kHz)
$R(33)$	$9P(2)-17\,522.841$	31 825 411.710	
$R(32)$	$9P(4)+16\,853.410$	31 811 962.083	
$R(30)$	$9P(4)-9928.356$	31 785 180.317	
$R(28)$	$9P(6)+12\,070.418$	31 758 554.205	
$R(26)$	$9P(6)-14\,400.993$	31 732 082.794	
$R(24)$	$9P(8)+8703.745$	31 705 765.167	
$R(22)$	$9P(8)-17\,460.978$	31 679 600.444	
$R(20)$	$9P(10)+6744.648$	31 653 588.032	
$R(12)$	$9P(14)+7019.453$	31 551 048.330	
$R(10)$	$9P(14)-18\,240.150$	31 525 788.727	
$R(8)$	$9P(16)+9241.222$	31 500 678.609	
$P(11)$	$9P(24)-15\,442.700$	31 257 804.449	26
$P(13)$	$9P(26)+17\,584.341$	31 234 345.644	
$P(16)$	$9P(26)-17\,317.243$	31 199 444.060	
$P(18)$	$9P(28)+16\,860.469$	31 176 368.632	12
$P(21)$	$9P(28)-17\,462.007$	31 142 046.156	
$P(23)$	$9P(30)+17\,867.587$	31 119 359.770	
$P(26)$	$9P(30)-15\,866.344$	31 085 625.839	15
$P(29)$	$9P(32)+9532.341$	31 052 250.406	
$P(31)$	$9P(32)-12\,516.562$	31 030 201.503	10
$P(34)$	$9P(34)+14\,243.151$	30 997 433.904	76

[a] ν_o center frequencies were obtained by fitting a second-derivative Gaussian function to the observed saturation-dip signals.
[b] CO_2 laser frequencies given by Maki et al. [9] were used.
[c] Frequency differences, $\Delta\nu$, between the present measurements and those reported by Fichoux et al. [5].

TABLE 1 Measured transition frequencies of the $2\nu_2$ overtone band of OCS

4 Measurement accuracy

The present measurements not only served to determine new OCS reference frequencies, but also to assess the accuracy of our spectrometer by comparison with the previous sub-Doppler data [5]. The experimental uncertainty in our frequency measurements arises from two main sources: the frequency accuracy of our locked CO_2 laser, and the accuracy of determination of the central frequency of the observed saturation dips in the spectral recordings.

The laser frequency is currently the most critical element in our overall precision. To ensure system stability, the MW synthesizer was always left in standby mode, and the laser and system electronics were turned on at least three hours before an experiment in order to reach thermal equilibrium. The key determinant of the laser accuracy is the error-correction signal generated by the servo loop, proportional to the first derivative of the 4.3-μm fluorescence Lamb dip. This signal can be characterized by the voltage spread ΔV_{pp} between the positive and negative first-derivative peaks, the corresponding difference $\Delta\nu_{pp}$ in laser frequency between the peaks, and the slope of the error signal at line center, $(dV/d\nu)_o$, which is the inverse of the tuning sensitivity.

Both systematic and random effects contribute to the CO_2 laser frequency uncertainty. Because the laser power has a rather broad maximum at the top of the gain curve, there is some uncertainty in adjusting the grating initially to tune to the center of the CO_2 line. Given the sensitivity of the high-resolution Evenson laser to the precise setting of the grating, the peak of the gain curve may thus be somewhat offset from line center, resulting in a sloping background at the position of the 4.3-μm Lamb dip. This leads to a DC shift in the first-derivative error-correction voltage so produces an asymmetry between the upper and lower peak heights and a systematic frequency offset from the true center of the CO_2 line [6, 10]. Similar effects might also arise from the presence of higher modes and/or a skewing of the gain curve due to slight misalignment of the laser cavity [10]. Therefore, to minimize any such frequency offset, we adopted the following procedure prior to the measurement of each OCS line. First, we located the approximate center of the Lamb dip by varying the PZT voltage, and maximized the laser power by adjusting the grating while monitoring the laser beam with a power meter. We then blocked the beam and zeroed the error voltage to remove any instrumental offsets arising from the lock-in circuitry. Next, we tuned back and forth through the Lamb dip with the laser beam unblocked to check for asymmetry in the error signal, and carefully readjusted the grating as necessary in order to remove any asymmetry and bring the center of the Lamb dip to zero volts as closely as possible given the noise on the signal. From our observations of meter readings of the error-correction signal, we estimate that any remaining systematic deviation from zero after this procedure would be no more than 4% of ΔV_{pp}, the peak-to-peak spread in the error voltage.

The random contributions to the laser frequency uncertainty originate from noise in the error-correction electronics and fluorescence signal, and mechanical and thermal fluctuations in the laser cavity. To assess their magnitude, we monitored the open-loop error-signal voltage fluctuations for the unlocked laser over a period of several minutes, and ob-

served free-running peak-to-peak short-term noise of about 10% of ΔV_{pp}, plus a slower back-and-forth drift of around 20% of ΔV_{pp}. When the locking loop was closed, the frequency stability tightened up, and the peak-to-peak fluctuations dropped below 5% of ΔV_{pp}, corresponding to a root-mean-square (rms) variation of under 2%.

We then carried out a calibration experiment to determine the frequency separation $\Delta\nu_{pp}$ between the peaks of the 4.3-μm Lamb dip in order to convert from % of ΔV_{pp} to absolute frequency deviations. As a reference marker, we used the saturation dip for the strong $Q(8)4A\ v_t = 0$; CH_3OH transition, reported at 1033.78448 cm^{-1} in the methanol C–O stretching Q branch [11], which is accessible in the upper sideband of the $9P(34)$ CO_2 line. First, we tuned the free-running laser to the upper peak of the 4.3-μm Lamb dip and ran a scan of the reference dip, obtaining a center frequency of 8898.59(2) MHz. Then, we tuned the laser down to the lower 4.3-μm peak and repeated the scan, now obtaining a frequency of 8897.68(2) MHz. The difference of 0.91(3) MHz is then directly equal to $\Delta\nu_{pp}$. As a check, we also tuned the laser to the center of the 4.3-μm Lamb dip, closed the servo loop, and ran a third scan with the laser locked. Here, we obtained a frequency of 8898.12(2) MHz, which does equal the average of the values at the upper and lower 4.3-μm peaks to within our measurement uncertainty. (As a useful by-product of the calibration experiment, this result yields a precise wavenumber of 1033.784808(1) cm^{-1} for the reference CH_3OH transition, slightly higher than the Fourier transform value in [11].)

Knowing $\Delta\nu_{pp}$ for the first-derivative locking signal, we can now quantify the frequency shifts corresponding to the observed % voltage deviations. For a small voltage excursion δV, the corresponding frequency shift $\delta\nu$ will be given by δV divided by the slope of the error correction curve $(dV/d\nu)_o$ at line center. This slope is simply the second derivative of the Lamb dip signal, so can be calculated explicitly for a specific line shape, as can the difference ΔV_{pp} between the first derivative peaks at frequency offsets $\pm\Delta\nu_{pp}/2$. For a Gaussian error signal profile, (1) leads to the results

$$\Delta V_{pp} = G'(-\Delta\nu_{pp}/2) - G'(+\Delta\nu_{pp}/2) = A[16/\pi\Delta\nu_{pp}^4]^{1/2}\exp(-1/2) \quad (2)$$

$$\therefore G''(\nu_o) = -[\Delta V_{pp}/\Delta\nu_{pp}]\exp(1/2) \quad (3)$$

$$\therefore \delta\nu = \delta V/G''(\nu_o) = [\delta V/\Delta V_{pp}]\Delta\nu_{pp}\exp(-1/2) = 0.6065\Delta\nu_{pp}[\delta V/\Delta V_{pp}]. \quad (4)$$

Thus, for our measured value of 0.91 MHz for $\Delta\nu_{pp}$ and the estimated $[\delta V/\Delta V_{pp}]$ of 2% in rms noise fluctuations, we obtain rms random frequency variations of ±11.0 kHz for a Gaussian shape. (For a Lorentzian profile, the numerical factor in (4) would be 0.5625 giving ±10.2 kHz rms variation, hence the result is not very sensitive to the exact line shape.) From (4), the possible systematic offset from line center of up to 4% of ΔV_{pp} associated with Lamb-dip asymmetry will add a further frequency uncertainty of up to ±22 kHz. Thus, taking the conservative view and simply adding the random and systematic contributions, we then obtain an overall estimate of ±33 kHz for the frequency accuracy of our locked CO_2 laser.

The precision with which the OCS line parameters can be determined by fitting to the observed line profiles is governed both by the signal-to-noise (S/N) ratio and by any distortions to the spectral line shapes. Important factors include variations in sideband power as the MW frequency is scanned (due to standing waves in the microwave circuitry or optical fringing in the beam path), and noise due to fluctuations in alignment arising from mechanical vibrations. Because the observed S/N ratios were fairly low for the relatively weak overtone OCS lines, noise fluctuations could act to distort the $2f$ line profiles and contribute to uncertainty in the line center frequencies. In order to reduce these effects, we repeated the observations several times for each line, scanning both upward and downward in frequency. The scatter in our repeated measurements corresponded to an rms statistical deviation δf of about ±15 kHz. Note, however, that this in fact includes the effects of the random laser fluctuations, since any change in laser frequency will also change the measured sideband frequency. Therefore, the overall uncertainty in our OCS measurements, adding the rms random variations of ±15 kHz to the possible systematic shifts of ±22 kHz, is estimated to be ±37 kHz.

The deviations in the last column of Table 1 support this uncertainty estimation. Our results for the $P(11)$, $P(18)$, $P(26)$, and $P(31)$ OCS lines are in good agreement with the frequencies measured earlier with ±20 kHz accuracy by Fichoux et al. [5], although our frequency for the $P(34)$ line is 76 kHz higher than theirs, for unknown reasons. Fichoux et al. also reported frequency predictions for the OCS lines, based on an extensive global fit to the known data [5]. The standard deviation of our 21 measurements relative to the predictions is 28.7 kHz, consistent with our ±37 kHz estimate, although our experimental frequencies are slightly higher on average.

5 Conclusions

In this work, with the broader frequency coverage of our CO_2-laser/microwave-sideband saturation-dip spectrometer, we have added 16 further sub-Doppler $2\nu_2$ measurements to the previous data set of 20 precise reference frequencies for the $2\nu_2$ and $3\nu_2 - \nu_2$ bands of OCS in the 10-μm region. From observations of the error signal characteristics of our laser-locking system and a calibration experiment using a CH_3OH reference line, we have determined the absolute accuracy of our new frequencies to be of the order of ±37 kHz. Comparative test measurements on previously known transitions support this estimate, as does the agreement of our new data with the OCS frequencies predicted by Fichoux et al. from global fit calculations [5]. Our present accuracy for OCS measurements appears to be significantly better than obtained in our earlier Lamb-dip results for CH_3OH lines [1]. This difference may be associated with the high line density in the CH_3OH spectrum, in which it is difficult to establish the true zero-absorption level against a dense background of weak lines as opposed to the well-isolated transitions in the comparatively sparse OCS spectrum. A similar difference was found previously for tunable far-IR (TuFIR) measurements, in which frequencies in the well-resolved CO spectrum could be measured with an accuracy of order ±20 kHz [12] whereas uncertainties in the dense methanol spectrum appeared to be rather higher at ±100 or ±200 kHz [13, 14].

Our current study was focused on the measurement of lines of the $2\nu_2$ overtone. Weaker $3\nu_2 - \nu_2$ hot band transitions in this region were also searched for but without success, most likely due to the low population at room temperature. In contrast, Fichoux et al. [5] used a heated cell and were able to observe a number of the hot band transitions.

In future, we will seek to improve the accuracy of our measurements by detecting in $3f$ mode at the third harmonic of the modulation signal in order to reduce further any background standing-wave effects. Locking the laser to the third harmonic of the 4.3-μm fluorescence would also reduce any systematic shifts due to Lamb-dip asymmetry [10]. As well, we plan to improve the spectrometer sensitivity by introducing a polarizing beamsplitter at the entrance to the absorption cell followed by a quarter-wave plate. The polarization of the returning beam will thereby be rotated by 90° and a significantly larger fraction will be reflected off the beamsplitter, increasing the signal at the detector and enhancing the S/N ratio. We hope then to be able to extend our measurements to additional low-J and high-J lines of the $2\nu_2$ overtone as well as the $3\nu_2 - \nu_2$ hot band of OCS to further enlarge the data set of standard reference frequencies.

ACKNOWLEDGEMENTS We are pleased to acknowledge financial support from the Natural Sciences and Engineering Research Council of Canada and the Canadian Institute for Photonic Innovations (CIPI) through the national Networks of Centres of Excellence Programme. M.Y.T. acknowledges partial support from the Russian Foundation for Basic Research and the Russian Ministry of Industry, Science and Technologies. We thank Profs. H. Odashima, F. Matsushima, S. Tsunekawa, K. Takagi, and the members of the Toyama laser spectroscopy group for their valuable inputs to our CO_2-laser/microwave-sideband system.

REFERENCES

1 Z.-D. Sun, Q. Liu, R.M. Lees, L.-H. Xu, M.Yu. Tretyakov, V.V. Dorovskikh: "Dual-ModeCO_2-Laser/Microwave-Sideband Spectrometer with Broadband and Saturation Dip Detection for CH_3OH", submitted to Rev. Sci. Instrum., in print
2 Z.-D. Sun, R.M. Lees, L.-H. Xu, M.Yu. Tretyakov, I. Yakovlev: Int. J. Infrared Millimeter Waves **23**, 1557 (2002)
3 K.M. Evenson, C.-C. Chou, B.W. Bach, K.G. Bach: IEEE J. Quantum Electron. **30**, 1187 (1994)
4 P.K. Cheo: IEEE J. Quantum Electron. **QE-20**, 700 (1984)
5 H. Fichoux, E. Rusinek, M. Khelkhal, J. Legrand, F. Herlemont, A. Fayt: J. Mol. Spectrosc. **189**, 249 (1998)
6 A.G. Maki, J.S. Wells: *Wavenumber Calibration Tables from Heterodyne Frequency Measurements* (National Institute of Standards and Technology Special Publication 821, U.S. Department of Commerce, Washington, DC 1991) and references therein
7 C. Freed, A. Javan: Appl. Phys. Lett. **17**, 53 (1970)
8 G. Duxbury: private communication
9 A.G. Maki, C.-C. Chou, K.M. Evenson, L.R. Zink, J.-T. Shy: J. Mol. Spectrosc. **167**, 211 (1994)
10 H. Odashima, M. Tachikawa, L.R. Zink, K.M. Evenson: J. Mol. Spectrosc. **188**, 245 (1998)
11 G. Moruzzi, B.P. Winnewisser, M. Winnewisser, I. Mukhopadhyay, F. Strumia: *Microwave, Infrared and Laser Transitions of Methanol* (CRC Press, Boca Raton, FL 1995)
12 T.D. Varberg, K.M. Evenson: IEEE Trans. Instrum. Meas. **42**, 412 (1993)
13 H. Odashima, F. Matsushima, K. Nagai, S. Tsunekawa, K. Takagi: J. Mol. Spectrosc. **173**, 404 (1995)
14 L.-H. Xu, J.T. Hougen: J. Mol. Spectrosc. **173**, 540 (1995)